Effect of boron doping on grain boundary cohesion in technically pure molybdenum investigated via meso-scale three-point-bending tests

International Journal of Refractory Metals and Hard Materials 113 (2023) 106173

Contents lists available at ScienceDirect

International Journal of Refractory Metals and Hard Materials

journal homepage: www.elsevier.com/locate/IJRMHM

Effect of boron doping on grain boundary cohesion in technically pure molybdenum investigated via meso-scale three-point-bending tests

S. Jakob [a,b], A. Hohenwarter [a], A. Lorich [c], W. Knabl [c], R. Pippan [d], H. Clemens [a], V. Maier-Kiener [a,*]

[a] Department of Materials Science, Montanuniversität Leoben, Leoben 8700, Austria
[b] Department of Physics, Chalmers University of Technology, Göteborg 412 96, Sweden
[c] Plansee SE, Reutte 6600, Austria
[d] Erich Schmid Institute of Materials Science, Austrian Academy of Sciences, Leoben 8700, Austria

ARTICLE INFO

Keywords:
Molybdenum
Segregation engineering
Grain boundaries
Interface cohesion
Atom probe tomography

ABSTRACT

Molybdenum has numerous advantageous functional and high-temperature properties. However, plastic deformation as well as structural applications are limited due to a propensity for brittle, intercrystalline failure, especially at low temperatures. It is well known that oxygen segregations have a detrimental effect, whereas it is assessed that carbon and/or boron have a beneficial effect on grain boundary cohesion. An advanced approach for the improvement of these interfaces is segregation engineering, e.g. the addition of cohesion enhancing elements segregating to the grain boundaries. To investigate early stages of crack formation, three-point bending tests on recrystallized commercially pure and boron micro-doped molybdenum were conducted between −28 °C and room temperature. The tensile-loaded top surface of the specimens was examined post-mortem close to the final fracture area via scanning electron microscopy. The occurring separations of grains are investigated for distinct features and the chemical composition of the interface is complementary measured by atom probe tomography.

1. Introduction

The demand for high-performance materials with a combination of functional and structural properties is ever increasing. The refractory metal Mo offers a unique set of properties due to its high melting point, its mechanical strength up to elevated temperatures as well as its high thermal and electrical conductivity in combination with a low thermal expansion coefficient. The broad field of applications include medical, lighting and electronic technologies [1]. However, there is depending on the processing state one limitation for structural applications of technically pure Mo, which is a low deformability at room temperature (RT). Especially in the recrystallized state, Mo is prone to fail in an intergranular manner. Beside the high brittle-to-ductile transition temperature, the inherently weak grain boundaries (GBs) [2–4] and detrimental segregations, e.g. O, present at these boundaries are the cause of this behavior [5–7]. Nevertheless, there are other elements such as C and/or B which are assessed to have a beneficial effect on interface cohesion [8–10]. These elements can therefore be used to tailor the strength of the interfaces by deliberately introducing doping elements, an approach known as segregation engineering [11,12].

The obvious defect initiation sites in single-phase materials are the GBs [13]. At these interfaces dislocation movement is generally impeded and consequently local strains increase [14–17]. If a geometry change on this local scale cannot be accommodated, voids or micro-cracks nucleate and de-cohesion of the material occurs [18]. To examine the damage nucleation, instable crack propagation should be avoided. Testing in bending configuration offers the possibility to load the sample with a stress and strain gradient over the sample thickness. Therefore, crack initiation should start at the highest loaded extreme fibre and the driving force for crack propagation should be reduced [19]. In this study, three-point-bending experiments were carried out on samples made from technically pure and B micro-doped Mo to elucidate the onset of fracture after plastic deformation.

2. Materials and methods

The samples were powder-metallurgically produced by Plansee SE (Reutte, Austria) and rolled to different thicknesses, labelled as plate and

* Corresponding author.
E-mail address: verena.maier-kiener@unileoben.ac.at (V. Maier-Kiener).

https://doi.org/10.1016/j.ijrmhm.2023.106173
Received 29 September 2022; Received in revised form 23 February 2023; Accepted 27 February 2023
Available online 2 March 2023

Table 1
Concentrations of accompanying elements in technically pure Mo sheet and B micro-doped Mo plate; # concentration in the sintered ingot (pre-material for sheet and plate). Concentrations determined via: * inductively coupled plasma - optical emission spectrometry, ** combustion analyses, *** carrier-gas analyses.

Element	Pure Mo [µg/g]	B-doped Mo [µg/g]
B*	< 5	10
C**	5	12
O***	20	9
N***	< 5	< 5
P*	< 10	< 10#

sheet. One material is technically pure Mo, the other has B as a dopant, added in small amounts as described in [20]. The concentrations of important accompanying elements in the recrystallized specimens are summarized in Table 1. The variation and differences of impurities are within expected ranges.

Samples with dimensions of 12 × 4 × 1 mm^3 were cut and one surface was ground and polished with SiC abrasive paper and 3 µm diamond suspension. Afterwards, a final electro-polishing step for 70 s with 25 V in 12.5 vol.-% H_2SO_4 in ethanol removed the deformation layer. Three-point-bending experiments were conducted between RT and − 28 °C on a Kammrath and Weiß GmbH (Dortmund, Germany) bending module in a cooling chamber. The deformation velocity was set to 5 µm/s and the sample was loaded until failure or a maximum displacement of 3000 µm, corresponding to a bending angle of about 90°.

Electron backscatter diffraction (EBSD) as well as atom probe tomography (APT) tip preparation were carried out using a FEI 3D Dual-Beam workstation (Thermo Fisher Scientific, Waltham, USA) equipped with an EDAX Hikari XP EBSD system (AMETEK Materials Analysis Division, Mahwah, USA). A Tescan CLARA field-emission scanning electron microscope (SEM) (TESCAN ORSAY HOLDINGS, a.s., Brno, Czech Republic) was used to capture micrographs of the tensile-loaded sample surface. The APT tips were prepared by the lift-out technique as described in [21] and measured on a CAMECA LEAP 3000X HR (AMATEK Materials Analysis Division). Measurement parameters were a laser energy of 0.6 nJ at 250 kHz, 60 K temperature, and a target evaporation of 0.5%. The software IVAS 3.6.14 was used for the reconstruction and analysis of APT data.

3. Results

The two material variants were subjected to the same rolling

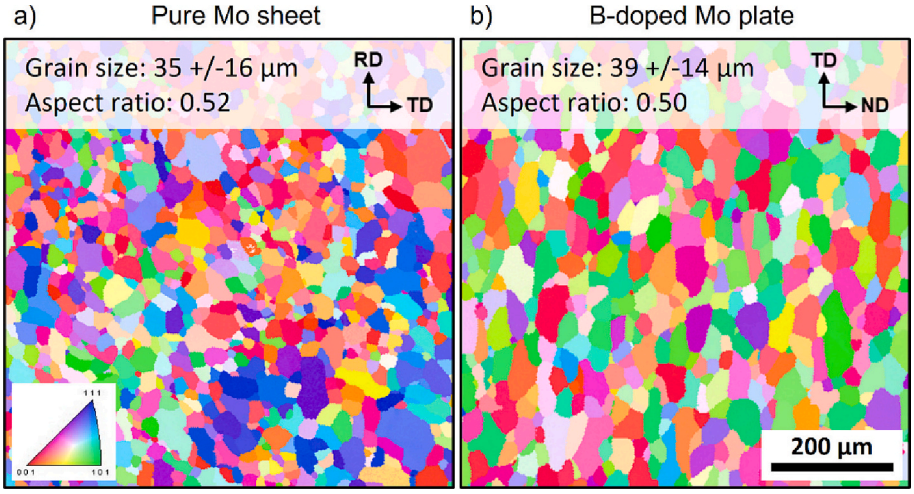

Fig. 1. Inverse pole figure maps of (a) pure Mo sheet and (b) B-doped Mo plate material with grain sizes calculated as equivalent diameters. The loading direction during bending experiments is in the horizontal direction (see text). RD…rolling direction, TD…transverse direction and ND…normal direction.

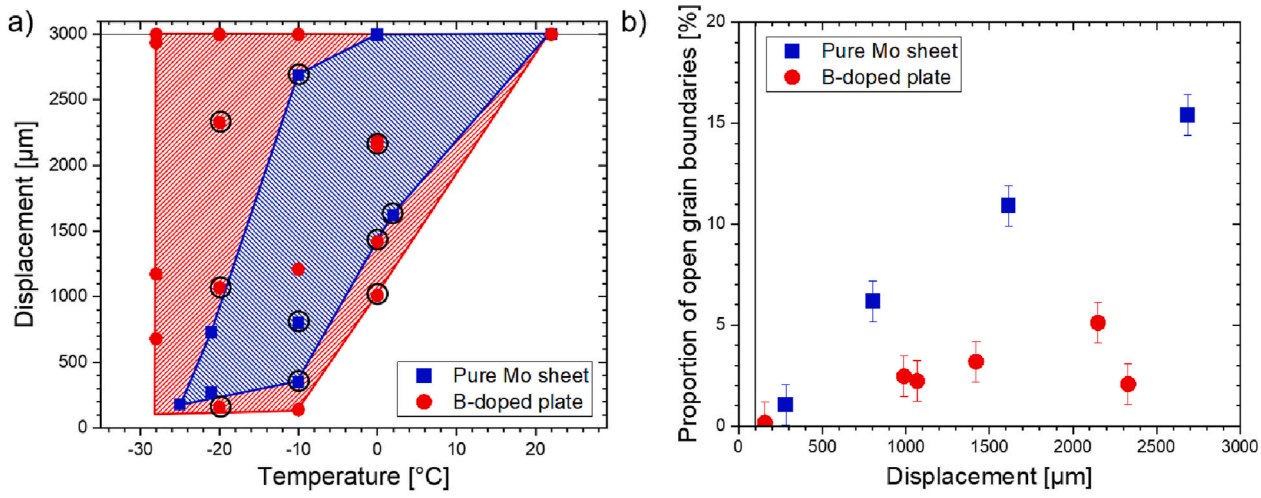

Fig. 2. a) Endured displacement as a function of temperature during bending for the two material variants. Samples indicated by circles were chosen for crack length analysis; b) proportion of intergranular cracks in relation to the overall GB length as a function of displacement until failure.

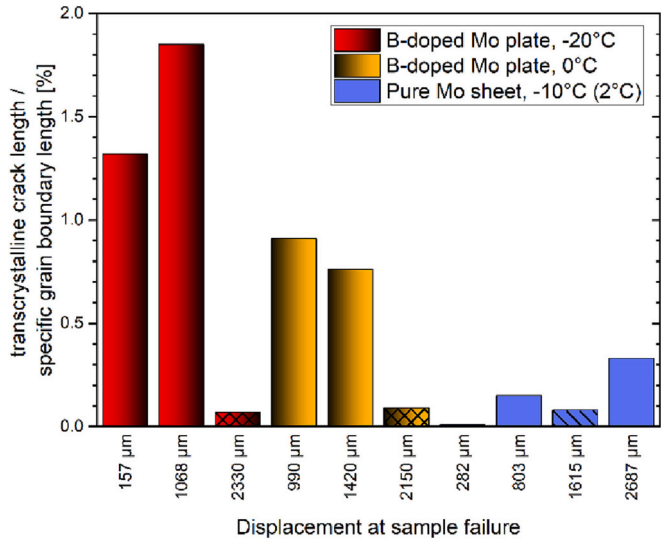

Fig. 3. The amount of transcrystalline cracks in proportion to the GB length is displayed for the analyzed samples. Cross-hatched bars indicate the two samples, which were unloaded after a significant load drop during bending.

procedure and the microstructures were analyzed by EBSD. A thourough investigation of microstructure and texture is documented in [22]. The grain sizes of pure Mo sheet (35 +/− 16 µm) and B-doped Mo plate (39 +/− 14 µm) are almost identical as can be seen in Fig. 1. Therefore these two sample variants were compared. The normal direction is most prone to separations and hence was chosen as the loading direction for samples from plate material. Due to the thinner specimens in case of sheet material, these samples were loaded in the transverse direction.

Three-point-bending test were carried out between −28 °C and RT until catastrophic failure of the sample or a significant load drop was evident during the experiment. Fig. 2a displays the displacement of each specimen as a function of test temperature. The shaded area indicates the scatter of different samples of one material variant. Pure Mo sheet material clearly displays the brittle-to-ductile transition, whereas B-doped Mo plate samples show larger variance, even at the lowest temperature of −28 °C. The circular markings indicate samples chosen for SEM analysis. The tensile-loaded surface near the final fracture plane was imaged post-mortem in backscattered electron contrast. The length of cracks was measured with the image processing software ImageJ [23] and put into relation to the overall GB length of the investigated area (for more detail see [22]). The calculated relative proportions of intergranular cracks are displayed in Fig. 2b. Samples from pure Mo sheet show the expected trend of higher relative crack length in accordance with increasing endured deformation before final fracture. The sample, which failed after 2687 µm bending displacement, recorded 15.4% separated GBs. The B-doped Mo plate specimens display the same trend of higher proportion of intergranular cracks with greater deformation up to a maximum of 5.1% of open GBs. However, the two B-doped samples with the highest displacement until failure were unloaded after a significant load drop in the test record. This is indicative of significant crack propagation in the microstructure without immediate fracture of the whole sample.

Beside the investigation of intercrystalline separations, the length of transcrystalline fracture was also recorded. Fig. 3 shows the amount of transgranular cracks in relation to the GB length. The B-doped samples show comparatively higher amount of transgranular separations compared to pure Mo. The two samples loaded to 2330 µm and 2150 µm (cross-hatched bars in Fig. 3) were unloaded after a significant load drop and do not show extensive transcrystalline separations. The samples with catastrophic failure are grouped according to the test temperature. The amount of transgranular cracks is on average 1.6% for samples tested at −20 °C compared to 0.8% at 0 °C. Between the pure Mo sheet samples, the amount of transgranular cracks are higher with increasing deformation up to 0.33%. The sample tested at 2 °C is shown as hatched bar in Fig. 3 and displays lower transgranular separations.

In order to evaluate the presence of segregations at the GB, APT measurements were conducted on both pure and B-doped Mo. Fig. 4a displays the reconstruction of one successful measurement of doped material with B and Mo atoms visible. The displayed region of interest was used for the calculation of the 1D-concentration profiles shown in Fig. 4b. The interfacial excess values can be calculated with the use of ladder-diagrams as demostrated in [24,25]. The B-doped material exhibits increased segregation of B and C (>2 atoms/nm^2), whereas the highest interfacial excess value in pure Mo is P with 0.35 atoms/nm^2 accompanied by other expected impurities for technically pure Mo [5].

4. Discussion

During bending the loading above the elastic limit results in the activation of dislocation sources within the grains and at the GBs. With increasing deformation the dislocations are pushed towards the generally impenetrable GBs [15,26]. If the resulting stress of the accumulated dislocations exceeds the cohesive strength of the GB before additional deformation in the neighboring grain is enabled, the boundary separates resulting in a GB crack [18,27,28]. After initiation, the crack follows the path of least resistance as long as enough driving force is provided. The

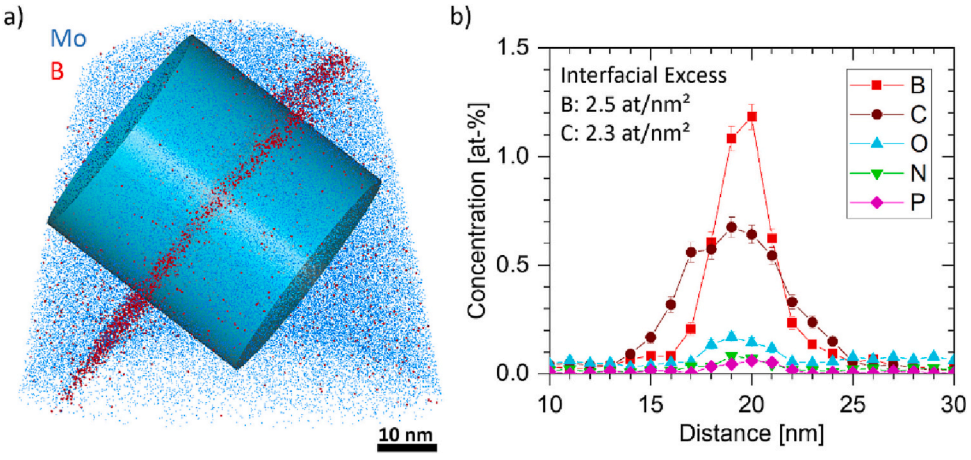

Fig. 4. a) Reconstruction of a GB from B-doped material measured by APT. Only Mo and B atoms are shown; b) 1D-concentration profile of the region of interest shown in (a). For more details see text.

test arrangement in bending mode results in a stress and strain gradient within the samples. Therefore, several GBs separate at the tensile-loaded extreme fibre without immediate fracture of the whole sample. Only when one of these cracks reach a critical size, the bending sample fails in catastrophic manner. It is noteworthy that the final fracture plane is intercrystalline for pure Mo and transcrystalline in the case of B-doped material. This is consistent with experiments of doped sintered parts as shown in [12]. Nevertheless, the presence of intercrystalline separations in both material variants is proof that the damage initiation happens at the GBs. Only further crack propagation favors different paths for the two materials.

After bending, the tensile-loaded top surface of the samples were investigated by SEM micrographs. The separations of GBs near the final fracture plane give an indication of how readily damage nucleates for the two sample material variants. The length of open GBs in regard to the overall GB length of the investigated surface area gives, therefore, a comparable and quantitative measure of the propensity to GB failure. Both variants show the expected trend towards higher amount of separated GBs with greater bending displacement. However, the values for B-doped material are widely reduced. The proportions of transgranular separations also show distinct differences between the material variants. B-doped material experiences a higher amount of transgranular separations than pure Mo. The two samples loaded to the highest bending displacements suffered a significant load drop during the experiment. This corresponds to a notable crack extension and the samples were unloaded afterwards. As a consequence, the amount of GB cracks at the surface of the extreme fibre might be underestimated. The small amount of transcrystalline cracks in these two samples, however, indicate that the majority of transgranular separations appear at the moment of final catastrophic failure due to additional deformation during the propagation of the final crack. At the lower temperature of −20 °C more separations through the grains are present compared to samples tested at 0 °C. This might be caused by a reduced possibility to accommodate the pile up of dislocations at lower temperatures.

Since the two investigated material variants, pure Mo sheet and B-doped plate, have a comparable microstructure, the differences in fracture behavior predominately stem from the segregations at the GBs. Mo has intrinsically weak GBs as shown for example in atomistic simulations [4]. However, the presence of segregations play a crucial role. O has a detrimental effect and further weakens the interface [6]. On the contrary, B and also C are shown to improve cohesion [9,10,29]. Beside the already reported effect of change in fracture mode, our experiments show that also damage initiation is affected in a beneficial way. Due to the doping of B into technically pure Mo, the presence of GB separations is drastically reduced, as can be seen in Fig. 2b. The amount of GB cracks in relation to the overall GB length for the B-doped material is reduced to one third of pure Mo.

5. Conclusions

In this study, bending tests have been performed to initiate GB failure on the tensile-loaded surface of technically pure and B micro-doped Mo samples. The length of separations is recorded from SEM micrographs and put into relation to the overall GB length. This value gives a comparable and quantitative value for the propensity to intercrystalline damage nucleation. The proportion of relative GB crack length is higher the more bending deformation is endured. The presence of cohesion enhancing dopant elements like B reduces the separated GB length to one third compared to technically pure Mo. Transgranular separations are most prominent in B-doped material which fractured in catastrophic manner. On samples, which were unloaded after a significant load drop, only limited transgranular cracks are observed. This suggests that these transcrystalline cracks only appear during final fracture.

CRediT authorship contribution statement

S. Jakob: Conceptualization, Formal analysis, Investigation, Methodology, Visualization, Writing – original draft. **A. Hohenwarter:** Investigation, Methodology, Writing – review & editing. **A. Lorich:** Investigation, Validation, Writing – review & editing. **W. Knabl:** Project administration, Resources, Writing – review & editing. **R. Pippan:** Conceptualization, Validation, Writing – review & editing. **H. Clemens:** Validation, Resources, Writing – review & editing. **V. Maier-Kiener:** Conceptualization, Project administration, Supervision, Writing – review & editing.

Declaration of Competing Interest

The authors declare that they have no known competing financial interests or personal relationships that could have appeared to influence the work reported in this paper.

Data availability

Data will be made available on request.

References

[1] J.A. Shields (Ed.), Applications of Molybdenum Metal and its Alloys, Second edi, International Molybdenum Association (IMOA), London, UK, 2013.
[2] H. Kurishita, S. Kuba, H. Kubo, H. Yoshinaga, Trans. Japan Inst. Met. 26 (1985) 332–340.
[3] H. Kurishita, A. Ôishi, H. Kubo, H. Yoshinaga, Trans. Japan Inst. Met. 26 (1985) 341–352.
[4] D. Scheiber, R. Pippan, P. Puschnig, L. Romaner, Model. Simul. Mater. Sci. Eng. 24 (2016) 35013.
[5] K. Leitner, P.J. Felfer, D. Holec, J. Cairney, W. Knabl, A. Lorich, H. Clemens, S. Primig (née Babinsky), Mater. Des. 135 (2017) 204–212.
[6] A. Kumar, B.L. Eyre, Proc. R. Soc. A 370 (1980) 431–458.
[7] A.V. Krajnikov, F. Morito, V.N. Slyunyaev, Int. J. Refract. Met. Hard Mater. 15 (1997) 325–339.
[8] H. Lutz, F. Benesovsky, R. Kieffer, J. Less-Common Met. Less-Common Met. 16 (1968) 249–264.
[9] T. Kadokura, Y. Hiraoka, Y. Yamamoto, K. Okamoto, Mater. Trans. 51 (2010) 1296–1301.
[10] D. Scheiber, R. Pippan, P. Puschnig, L. Romaner, Model. Simul. Mater. Sci. Eng. 24 (2016).
[11] D. Raabe, M. Herbig, S. Sandlöbes, Y. Li, D. Tytko, M. Kuzmina, D. Ponge, P. P. Choi, Curr. Opin. Solid State Mater. Sci. 18 (2014) 253–261.
[12] K. Leitner, D. Lutz, W. Knabl, M. Eidenberger-Schober, K. Huber, A. Lorich, H. Clemens, V. Maier-Kiener (née Babinsky), Scr. Mater. 156 (2018) 60–63.
[13] T.R. Bieler, P. Eisenlohr, F. Roters, D. Kumar, D.E. Mason, M.A. Crimp, D. Raabe, Int. J. Plast. 25 (2009) 1655–1683.
[14] T.B. Britton, A.J. Wilkinson, Acta Mater. 60 (2012) 5773–5782.
[15] S. Kondo, T. Mitsuma, N. Shibata, Y. Ikuhara, Sci. Adv. 2 (2016).
[16] T. Ohmura, A.M. Minor, E.A. Stach, J.W. Morris, J. Mater. Res. 19 (2004) 3626–3632.
[17] S. Jakob, A. Leitner, A. Lorich, M. Eidenberger-Schober, W. Knabl, R. Pippan, H. Clemens, V. Maier-Kiener, Mater. Des. 182 (2019), 107998.
[18] T. Bieler, R.L. Goetz, S.L. Semiatin, Mater. Sci. Eng. A 405 (2005) 201–213.
[19] T.R. Bieler, S.C. Sutton, B.E. Dunlap, Z.A. Keith, P. Eisenlohr, M.A. Crimp, B. L. Boyce, JOM 66 (2014) 121–128.
[20] K. Huber, M. O'Sullivan, M. Eidenberger-Schober, R. Storf, Sintered Molybdenum Part, International Patent WO 2019/060932 A1, 2019.
[21] K. Babinsky, R. De Kloe, H. Clemens, S. Primig, Ultramicroscopy 144 (2014) 9–18.
[22] S. Jakob, A. Hohenwarter, A. Lorich, W. Knabl, R. Pippan, H. Clemens, V. Maier-Kiener, Mater. Des. 207 (2021), 109848.
[23] C.A. Schneider, W.S. Rasband, K.W. Eliceiri, Nat. Methods 9 (2012) 671–675.
[24] M. Thuvander, H.O. Andrén, Mater. Charact. 44 (2000) 87–100.
[25] B.W. Krakauer, D.N. Seidman, Phys. Rev. B 48 (1993) 6724–6727.
[26] J. Kacher, B.P. Eftink, B. Cui, I.M. Robertson, Curr. Opin. Solid State Mater. Sci. 18 (2014) 227–243.
[27] T.R. Bieler, A. Fallahi, B.C. Ng, D. Kumar, M.A. Crimp, B.A. Simkin, A. Zamiri, F. Pourboghrat, D.E. Mason, Intermetallics 13 (2005) 979–984.
[28] J.A. Querin, J.A. Schneider, M.F. Horstemeyer, Mater. Sci. Eng. A 463 (2007) 101–106.
[29] K. Leitner, D. Scheiber, S. Jakob, S. Primig, H. Clemens, E. Povoden-Karadeniz, L. Romaner, Mater. Des. 142 (2018) 36–43.